Renewable Energy 220 (2024) 119678

Contents lists available at ScienceDirect

Renewable Energy

journal homepage: www.elsevier.com/locate/renene

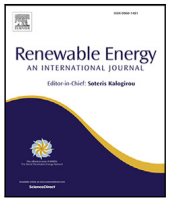

Long-term assessment of wave conditions and wave energy resource in the Arctic Ocean

Konstantinos Christakos [a,b,*], George Lavidas [c], Zhen Gao [a,d], Jan-Victor Björkqvist [b,e]

[a] Department of Marine Technology, Norwegian University of Science and Technology (NTNU), 7491 Trondheim, Norway
[b] Norwegian Meteorological Institute, Allégaten 70, 5007 Bergen, Norway
[c] Faculty of Civil Engineering and Geosciences, Delft University of Technology, Stevinweg 1, 2628 CN Delft, The Netherlands
[d] School of Naval Architecture, Ocean and Civil Engineering, Shanghai Jiao Tong University, 800 Dongchuan Road, 200240 Shanghai, China
[e] Finnish Meteorological Institute, Erik Palménin aukio 1, 00560 Helsinki, Finland

ARTICLE INFO

Keywords:
Waves
Energy
Extreme
Arctic
NORA3

ABSTRACT

It was recently shown that the Arctic has been warming much faster than the rest of the globe during the last decades. This warming has reduced the ice extent significantly, which will strongly impact the wave climate in the Arctic regions, thus affecting the design of marine structures, operations, and energy resources. This study focuses on the higher latitudes, and uses the advanced wave hindcast NORA3, which covers a big part of the North Atlantic and the whole Arctic Ocean, to analyze the spatio–temporal properties of wave height and wave energy flux during the last three decades. The most energetic waves in the Arctic Ocean are observed in the Greenland Sea and the Barents Sea. The study shows that the substantial diminishing of sea ice in the Arctic induces local and regional changes in both mean and extreme wave conditions. In the Arctic Ocean the changes in extreme wave height are more pronounced compared to changes in mean wave conditions. The results also indicate a strong positive trend in the extreme wave heights in the Arctic regions of the Barents Sea, the Kara Sea, the Laptev Sea, the East Siberian Sea, the Chukchi Sea, and the Beaufort Sea.

1. Introduction

Ocean renewable energy resources such as offshore wind, tides, and waves will play a vital role in carbon-free electricity production worldwide. The ocean provides an enormous amount of renewable energy that is nearly unexploited. The European Commission has identified the potential of the marine renewable energy sector. It has set ambitious targets with its Offshore Energy Strategy, aiming for ≥300 GW for offshore wind and 40 GW by ocean energies by 2050 [1]. These goals are even more critical now, as the energy crisis is driving costs up, and the need to utilize indigenous European renewable resources becomes demanding.

Historical data on wave conditions are crucial for developing renewable ocean projects, including the precise estimation of a renewable resource, the design of offshore structures, costs, and the planning of marine operations, including installation, decommissioning, and maintenance activities. Detailed knowledge of wave conditions is valuable, offering unique insights into energetic areas, accurate estimation of weather windows for marine operations, and precise analysis of the occurrence/magnitude of extreme conditions for designing safe structures.

There are several methods used to quantify the ocean's renewable energy resource, each with its distinct benefits and limitations [2]. Lavidas [3] introduced a novel index, SIWED, that accounts for the interactions of wave climate and wave energy converters, providing an unbiased approach that considers climate variability, survivability, and energy production. For applications of such methods, a long-term homogeneous dataset with ≤3 h intervals for at least ten years is needed to estimate ocean renewable energies characteristics correctly.

While wave buoys and in situ measurements are valuable, such techniques pose restrictions in spatial resolution and are often associated with costly sensors and maintenance operations. The use of numerical simulations offers a low-cost alternative to measurements. Altimeters are increasingly improving their reach; however, they still have significant limitations in the parameters they can reliably estimate (primarily significant wave height), and they are unreliable at nearshore locations and regions with complex orography [4].

Christakos et al. [5] mapped the potential wave energy and presented a spatiotemporal assessment of swell- and wind-sea-induced energy flux in the Nordic Seas using the NORA10 hindcast. The NORA10 hindcast has a spatial and temporal resolution at 10 km and 3 h. The

* Corresponding author at: Department of Marine Technology, Norwegian University of Science and Technology (NTNU), 7491 Trondheim, Norway.
E-mail address: konstantinos.christakos@ntnu.no (K. Christakos).

https://doi.org/10.1016/j.renene.2023.119678
Received 11 April 2023; Received in revised form 6 September 2023; Accepted 15 November 2023
Available online 17 November 2023

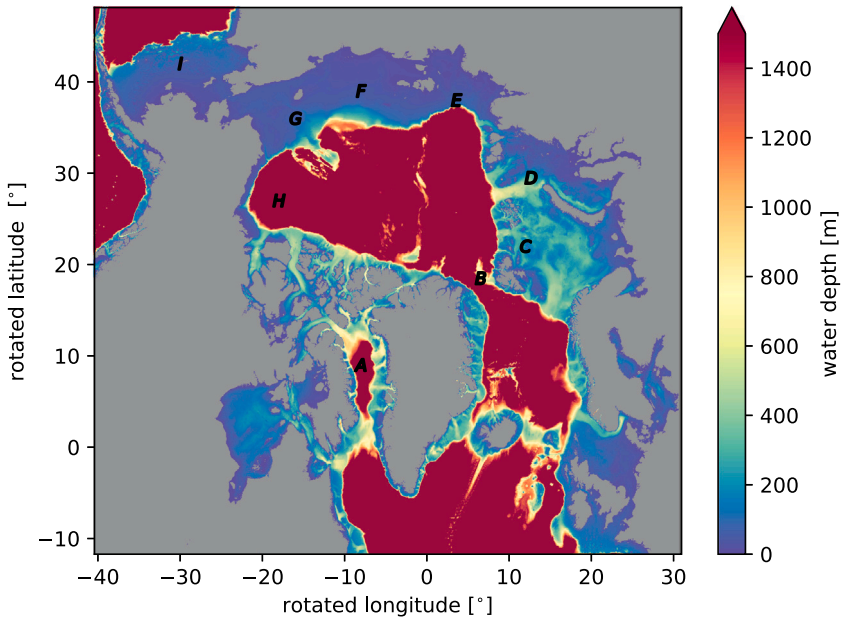

Fig. 1. Model domain and water depth in NORA3 with selected locations in the Arctic Ocean: A (Baffin Bay), B (Greenland Sea), C (Barents Sea), D (Kara Sea), E (Laptev Sea), F (East Siberian Sea), G (Chukchi Sea), H (Beaufort Sea), and I (Bering Sea). Gray color indicates land.

NORA10's model domain included a big part of the Northeast Atlantic but not the Arctic Ocean.

Our study presents spatio–temporal analyses of wave height and wave energy flux, focusing on the Arctic Ocean, a unit area with strong wave–ice interactions and significant changes in sea ice concentration during the last decades. This region needs to see more focus on developing marine renewable energies, and this work is amongst the few that identify the long-term changes and impacts on wave energy. The uniqueness of our approach is that we not only estimate the wave energy flux but also consider the long-term changes. The dataset we use for the analysis covers a big part of the North Atlantic and the Arctic Ocean with a high spatial (3 km × 3 km) and temporal (1 h) resolution. Using this hindcast, we investigate the average and extreme wave conditions during the period 1990–2019, identifying long-term trends due to changes in resource and ice conditions with a focus on higher latitudes. Various indices are used to unveil the true potential of wave energy in the region when usually the mean/average conditions are used. Our analysis goes beyond what is usually used and assists in identifying wave energy-rich areas, providing long-term advantages for marine renewable deployments.

This paper is organized as follows. Section 2 is dedicated to data and methods. Section 3 describes the results. Finally, the discussion and concluding remarks are given in Section 4.

2. Data and methods

2.1. NORA3

The NORA3 (NOrwegian Reanalysis Archive 3 km) is a long-term hindcast developed by the Norwegian Meteorological Institute, combining advanced atmospheric and wave modeling techniques. It has an atmospheric [6] and wave [7] model component. The wave component covers a large part of the North Atlantic and the Arctic Ocean, as illustrated in Fig. 1.

It is a dynamical downscaling (directional wave spectra at the boundaries) of the ERA5 reanalysis [8] data using winds from the 2.5-km AROME [9] for the Nordic Seas, and ERA5 wind for the rest of the domain to force the wave model WAM Cycle 4.7 (open-source WAM model [10–12]). Fields of daily ice concentration were provided by the ARC-MFC physical reanalysis system of the Copernicus Marine Service [13]. Xie et al. [14] assessed the quality of ARC-MFC in the Arctic region finding that sea ice concentration agrees well to satellite observations. The model uses physics based on "Source term package 4" (ST4) by Ardhuin et al. [15]. The spatial resolution is 3 km, and the output is provided with 1 h time interval. For realistic simulation of coastal waves, NORA3 uses a sub-grid scheme based on Tuomi et al. [16] that utilizes information from a high-resolution topography [17] to reduce the energy that propagates through partially land-covered grid points. NORA3 exhibits high-quality performance for both wind and wave conditions. As stated by Haakenstad et al. [6], NORA3 shows a clear improvement compared to ERA5 in the representation of surface winds over the ocean and a more realistic model activity than in ERA5 and NORA10. According to Breivik et al. [7], the significant wave height in NORA3 corresponds well to observations (in situ and altimeter) up to extreme wave conditions, and the zero-crossing period also shows a good agreement.

In addition to wave parameters, NORA3 hindcast includes output variables related to sea ice, such as thickness and concentration. These parameters have been statistically downscaled to the NORA3 grid. In the present study, we use the Sea Ice Concentration (SIC), also known as sea-ice area fraction, the grid cell's fractional sea ice coverage. It shows how much of a grid cell is covered with sea ice. SIC is often used as a climate change indicator in high latitudes. The SIC values range from 0 (no sea ice) to 1 (full sea ice coverage). There are several methods to account for the ice cover in wave models. The simplest one is to set a threshold of the SIC (e.g. 30%). If this threshold is exceeded, the grid point is momentarily excluded from calculations. This method was implemented by e.g. [18] in the Baltic Sea. A slightly more sophisticated method is to use similar sub-grid obstructions as for unresolved islands, following e.g. [19]. The differences in performance of these two methods have been compared by Tuomi et al. [20]. In NORA3, waves are allowed to propagate under the sea ice following the two layer model for wave dissipation in sea ice by Sutherland et al. [21].

2.2. Wave parameters

The significant wave height (H_s) and mean energy period (T_e) in NORA3 are estimated based on the spectral moments. The nth-order

moment of the density spectrum is given by

$$m_n = \int_0^{\infty}\int_0^{2\pi} f^n E(f,\theta)\, d\theta\, df, \tag{1}$$

where E is the variance density spectrum, f is the wave frequency and θ is the wave direction. The significant wave height and energy period are then defined as:

$$H_s = 4\sqrt{m_0}, \tag{2}$$

$$T_e = \frac{m_{-1}}{m_0}. \tag{3}$$

The wave energy flux (WEF) is given by:

$$WEF = \rho g \int_0^{\infty}\int_0^{2\pi} c_g E(f,\theta)\, d\theta\, df, \tag{4}$$

where ρ is the water density, g is the gravitational acceleration, and c_g is the water depth and frequency dependent group velocity. Assuming deep water conditions (valid for most of the NORA3 domain, Fig. 1), the wave energy flux in kW per meter of wave crest length (kW m^{-1}) is approximately estimated as:

$$WEF \approx 0.5 {H_s}^2 T_e. \tag{5}$$

We estimate the average values (arithmetic mean, denoted with a bar, e.g., $\overline{H_s}$) over a time period e.g., the overall period 1990–2019 or decades 1990s (1990–1999), 2000s (2000–2009), and 2010s (2010–2019s). There is no single best way to calculate wave statistics in partially ice-covered seas (see e.g. [18]), but here we present ice-included statistics. This is the most accurate way to calculate an overall change in the wave conditions, since the presence of the ice-cover has already been accounted for by the model. The extreme values are represented using the annual maximum (maximum value over a year) e.g., $H_{s,annual(max)}$.

2.3. Probability of exceedance

For certain operations (e.g., maintenance or installation), one might need to quantify the probability that different parameters exceed a given threshold value; in other words, the probability, P, of a variable X surpassing a reference level X_{ref}. Usually, availability, accessibility and weather windows are used as metric for assessing the potential and operational accessibility of a region [22,23]. Similarly, the probability of exceedance is estimated directly from the data as the fraction of hourly values exceeding the reference level, i.e.

$$P(X \geq X_{ref}) = \frac{N\left(\{X : X \geq X_{ref}\}\right)}{N\left(\{X\}\right)}, \tag{6}$$

where N denotes the number of elements in the set.

2.4. Trend

Linear regression is commonly used to estimate climate analyses' trends (slope). A linear regression model quantifies the amount of the linear relation between two variables; a dependent (y) and an independent (x) variable. The model can be expressed mathematically as

$$y = \alpha + \beta x \tag{7}$$

where α is the y-intercept and β is the slope (or trend).

We applied two methods to estimate α and β. The standard approach for calculating the slope of a linear regression line is based on the least-squares estimate (LSE). The method estimates y-intercept and the slope by minimizing the squared discrepancies between y and x and the slope is then given by

$$\beta_{LSE} = \frac{\sum_{i=1}^{N}(y_i - \overline{y})(x_i - \overline{x})}{\sum_{i=1}^{N}(x_i - \overline{x})^2}. \tag{8}$$

However, this method is sensitive to outliers. A more robust, non-parametric calculation of the slope was developed by Sen [24], and it is known as the Theil–Sen estimator or Sen's slope estimator. The Theil–Sen's slope is calculated as the median (M) from all slopes:

$$\beta_{TSE} = M\left\{\frac{y_j - y_i}{x_j - x_i} : x_i < x_j\right\}. \tag{9}$$

We used the Mann–Kendall test [25,26] at a confidence level of 99.5% for the estimation of β_{LSE} and β_{TSE}. We used the open-source Python package pyMannKendall [27] to calculate Theil–Sen's Slope Estimator and the confidence levels.

3. Results

3.1. Changes in sea ice concentration

Changes in ice concentration can explain significant differences in the wave parameters. We employ a certain concentration threshold to investigate the sea ice changes in the Arctic. We chose the threshold of 30%, which indicates open sea conditions (no sea ice). Changes in the probability of exceedance for the sea ice concentration ($P(SIC < 0.3)$) from 1990–2019 are illustrated in Fig. 2. The areas with the highest difference (up to ±25%) in $P(SIC < 0.30)$ between the 1990s(−)/2010s(+) and 1990–2019 are the East of Svalbard, West of Greenland, and the Chukchi Sea. The sea ice reduction over the three decades are also noticeable in Fig. A.1 which shows ice-free statistics of significant wave height.

3.2. Average wave height

The spatial variation of the $\overline{H_s}$ during the overall period 1990–2019 and the difference between the 1990s/2000s/2010s and 1990–2019 are shown in Fig. 3 for NORA3 domain.

The highest mean values in 1990–2019 for $\overline{H_s}$ is 3.5 m (see ice-free $\overline{H_s}$ in Fig. A.1 for 1990s, 2000s, 2010s), detected in the area South of Iceland and Northeast of Ireland. Lower values of $\overline{H_s}$ (up to 2.5 m) are observed in the North Sea, which is less exposed to high swell-type waves due to sheltering by the British Isles. The Norwegian Sea directly exposed to high waves from the North Atlantic Ocean shows $\overline{H_s}$ up to 3 m. The part of the Arctic Ocean with the highest waves is the Barents Sea and the Greenland Sea with $\overline{H_s}$ up to 2.5 m. Similar values of $\overline{H_s}$ (up to 2.5 m) are also observed in the Gulf of Alaska and the Bering Sea. The remaining part of the Arctic Ocean is characterized by low $\overline{H_s}$ (up to 0.5 m).

Between the three decades, we observe noticeable changes of $\overline{H_s}$ (up to 0.5 m) in the Arctic areas where the SIC changes are significant during the study period, i.e., Northeast of Svalbard, West of Greenland, and at the Chukchi Sea. In these areas, we detect a negative difference in wave height ($\overline{\Delta H_s} < 0$) between the 1990s and the overall period, while a positive difference ($\overline{\Delta H_s} > 0$) between the 2010s and the overall period.

The estimated trend (both β_{TSE} and β_{LSE}) of annual mean significant height ($H_{s,annual(mean)}$) from 1990 to 2019 is insignificant in the NORA3 domain (not shown).

3.3. Average wave energy flux

The spatial variation of the $\overline{WEF}$ during the period 1990–2019 and the difference between the 1990s/2000s/2010s and 1990–2019 are shown in Fig. 4 for NORA3 domain.

The highest mean values in 1990–2019 for $\overline{WEF}$ is up to 80 kW m^{-1}, detected in the South of Iceland and Northeast of Ireland. Lower values of $\overline{WEF}$ up to 40 kW m^{-1} are observed in the North Sea due to sheltering by the British Isles.

On the other hand, the Norwegian Sea with direct exposure to the North Atlantic Ocean shows higher values of $\overline{WEF}$ (up to 60 kW m^{-1}).

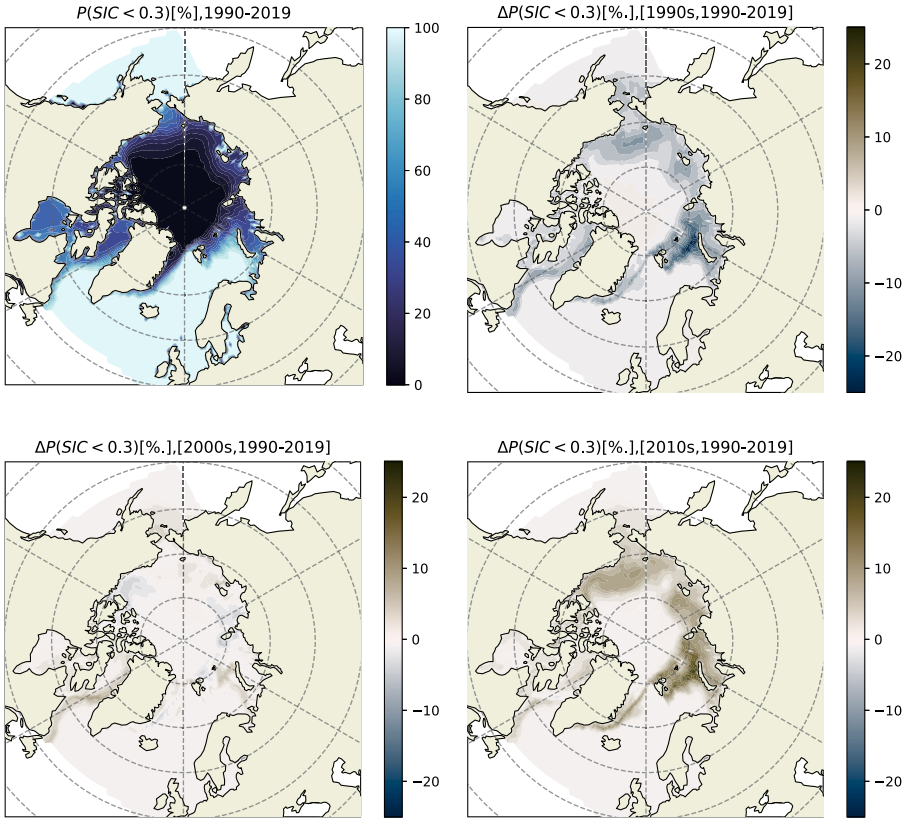

Fig. 2. $P(SIC < 0.3)$ for 1990–2019 and the difference $\Delta P(SIC < 0.3)$ between the 1990s/2000s/2010s and 1990–2019. The SIC lower than 0.3 indicates open water (no sea ice).

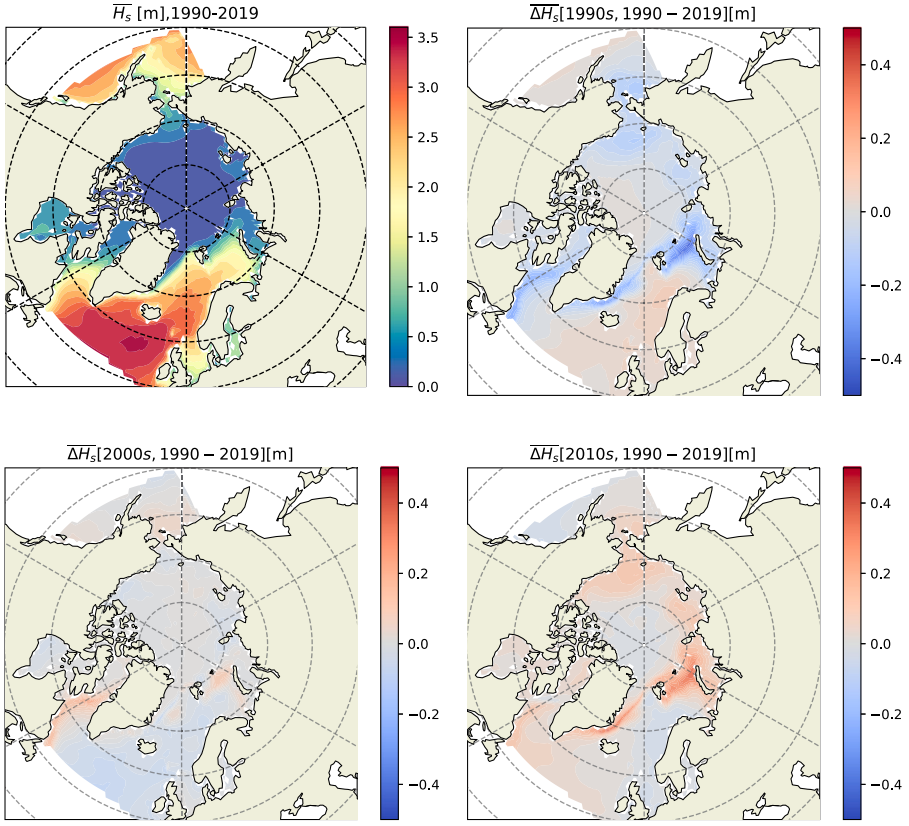

Fig. 3. Average significant wave height ($\overline{H_s}$) for 1990–2019 and the difference $\overline{\Delta H_s}$ between the 1990s/2000s/2010s and 1990–2019.

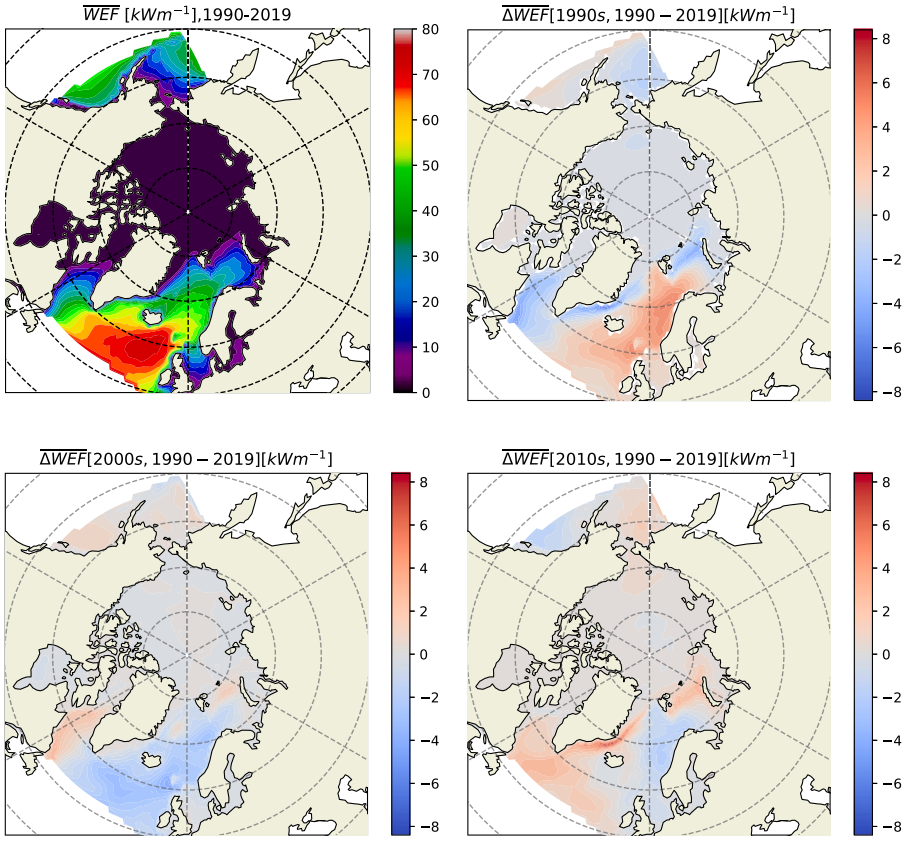

Fig. 4. Average wave energy flux ($\overline{WEF}$) for 1990–2019 and the difference $\overline{\Delta WEF}$ between the 1990s/2000s/2010s and 1990–2019.

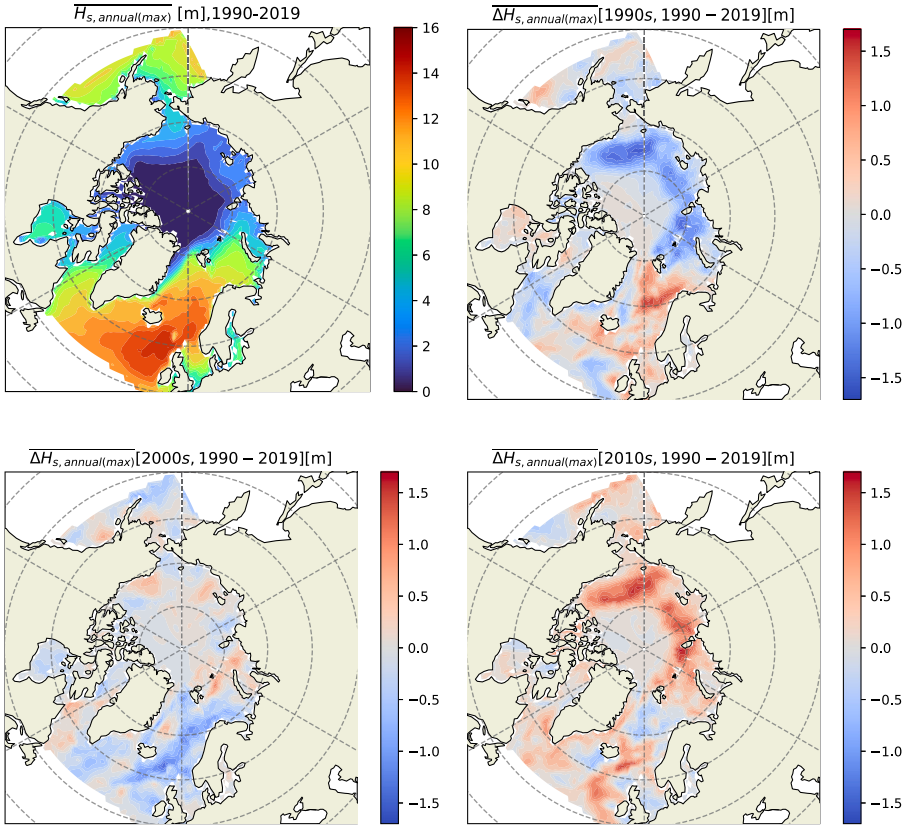

Fig. 5. Average annual maximum significant wave height ($\overline{H}_{s,annual(max)}$) for 1990–2019 and the difference $\overline{\Delta H}_{s,annual(max)}$ between the 1990s/2000s/2010s and 1990–2019.

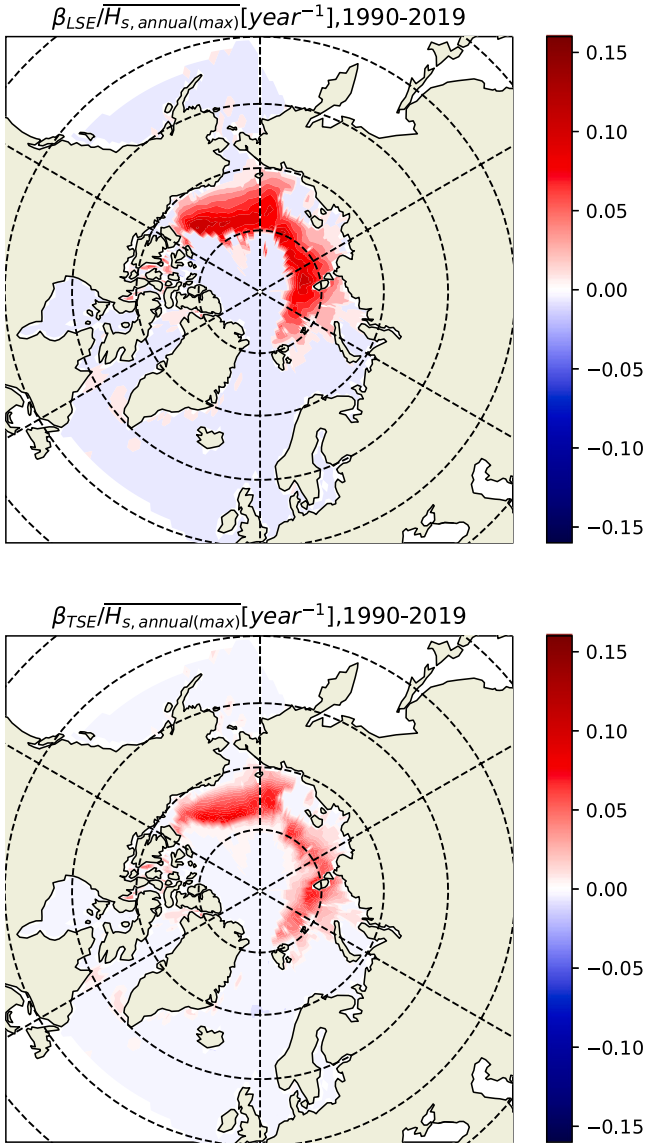

Fig. 6. Normalized β (trend) of annual maximum of significant wave height ($\overline{H}_{s,annual(max)}$) using the least-square estimator (LSE) and the Theil–Sen estimator (TSE) for the period January 1, 1990 to December 31, 2019.

The part of the Arctic Ocean with the highest $\overline{WEF}$ is the Barents Sea and the Greenland Sea with values up to 45 kW m^{-1}. Up to 40 kW m^{-1} $\overline{WEF}$ are also observed at the Gulf of Alaska and the Bering Sea. The remaining part of the Arctic Ocean is characterized by low $\overline{WEF}$ (up to 10 kW m^{-1}).

Between the three decades, we observe changes of up to ±8 kW m^{-1} in the Arctic areas, mainly in the Northeast of Svalbard and West of Greenland. Similar to H_s, we detect a negative difference of wave energy flux ($\overline{\Delta WEF} < 0$) between the 1990s and the overall period, while a positive difference ($\overline{\Delta WEF} > 0$) between the 2010s and the overall period.

The estimated trend (both β_{TSE} and β_{LSE}) of $\overline{WEF}$ from 1990 to 2019, again, is insignificant in the NORA3 domain (not shown).

3.4. Extreme wave height and wave energy flux

The spatial variation of the average annual maximum $\overline{H}_{s,annual(max)}$ and the difference $\overline{\Delta H}_{s,annual(max)}$ between the 1990s/2000s/2010s and 1990–2019 are shown in Fig. 5 for NORA3 domain (see Fig. A.1 for ice-free $\overline{H}_{s,annual(max)}$ for 1990s, 2000s, 2010s). Compared to mean values illustrated in Fig. 3, the annual maximum values show more pronounced anomalies in the Arctic Ocean with up to ±1.7 m difference between the 1990s(−)/2010s(+). The area North/Northeast of Great Britain has the highest $\overline{H}_{s,annual(max)}$ (14 m). Slightly lower values, i.e., $\overline{H}_{s,annual(max)}$ up to 12 m are observed in the Norwegian Sea. The part of the Arctic Ocean with the highest $\overline{H}_{s,annual(max)}$ (up to 10 m) is the Barents Sea, the Greenland Sea, the Gulf of Alaska, and the Beiring Sea. The remaining part of the Arctic Ocean is characterized by $\overline{H}_{s,annual(max)}$ up to 3 m.

3.5. Extreme wave height trend

To analyze further the change in the extreme wave heights over time, we estimated the trend (β) from 1990 to 2019 in the NORA3 domain using the least-square and the Theil–Sen estimators (Fig. 6). As expected, the two estimators show similar results, with the least-square method exhibiting higher values.

The results illustrate a strong trend in a crescent-shaped area from the North of Svalbard to the North of Alaska, including regions in the Barents Sea, the Kara Sea, the Laptev Sea, the East Siberian Sea, the Chukchi Sea, and the Beaufort Sea, (C – H locations in Fig. 1). A similar trend is also observed for annual maximum WEF (not shown).

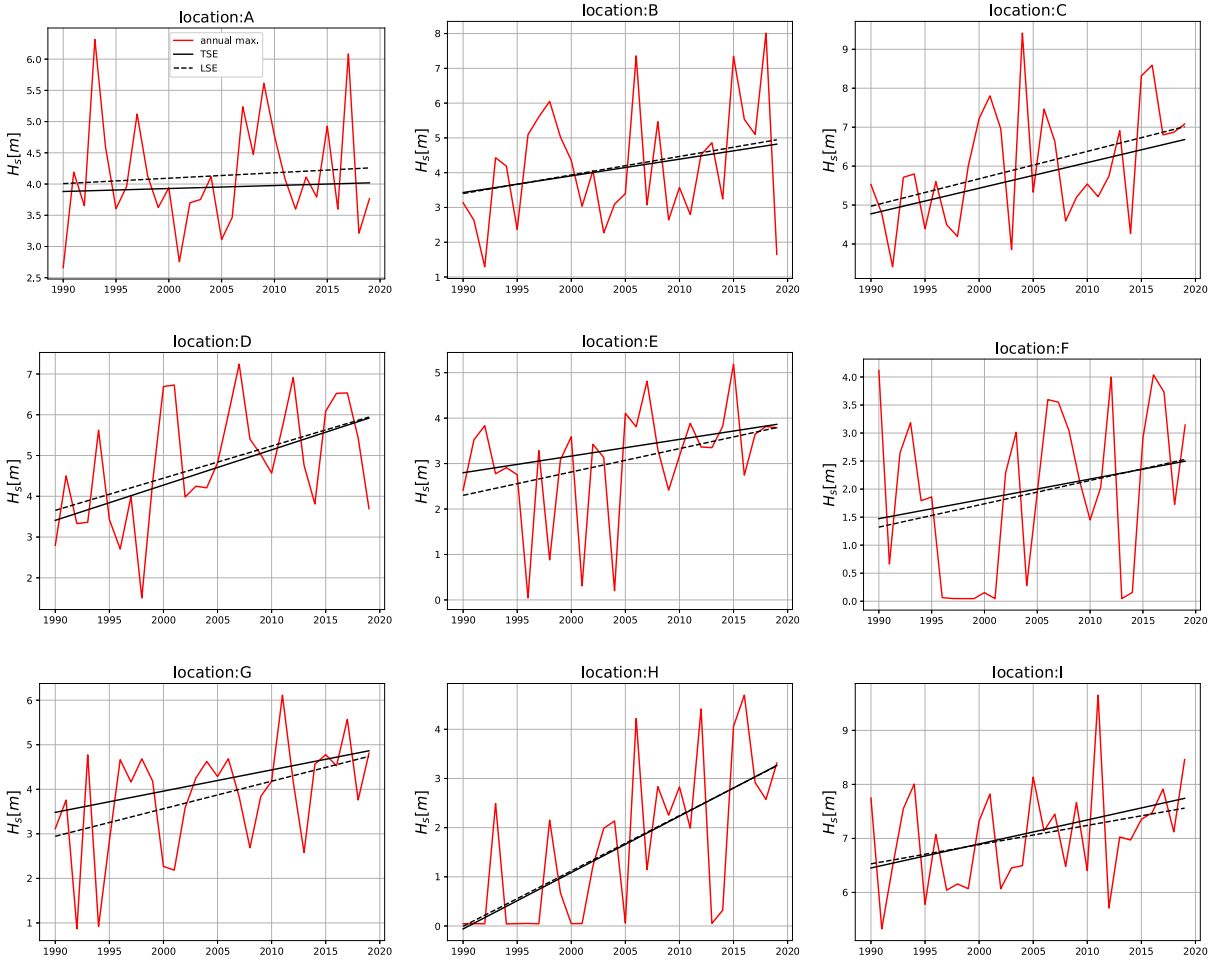

Fig. 7. Maximum annual significant wave height (H_s) for the period January 1, 1990, to December 31, 2019, at locations A-I. The line represents the linear fit on the annual maximum values using the Theil–Sen estimator (TSE, solid) and the least-square estimator (LSE, dashed).

Table 1
Trend, based on Theil–Sen estimator, of maximum annual significant wave height and wave energy flux for period January, 1990, to December 31, 2019, at locations A-I. Values correspond to trend lines in Figs. 7 and 8.

Location	$\beta_{TSE,Hs,annual(max)}$ [m year^{-1}]	$\beta_{TSE,WEFannual(max)}$ [kW (m year)$^{-1}$]
A (Baffin Bay)	0.00	0.85
B (Greenland Sea)	0.05	3.75
C (Barents Sea)	0.07	6.63
D (Kara Sea)	0.09	7.41
E (Laptev Sea)	0.04	0.95
F (East Siberian Sea)	0.04	0.52
G (Chukchi Sea)	0.05	2.88
H (Beaufort Sea)	0.11	1.16
I (Bering Sea)	0.04	2.00

For the selected locations in the Arctic Ocean (Fig. 1), we have plotted the actual time series of $H_{s,annual(max)}$ and $WEF_{annual(max)}$ for 1990–2019 and their trends in Figs. 7 and 8, respectively. All locations (A–I) show positive values of β for both TSE and LSE methods. The Greenland Sea, the Barents Sea, and the Kara Sea show high β for both wave height and wave energy flux (Table 1).

3.6. Exceedance probability of wave height and wave energy flux

The average exceedance probability of significant wave height for levels 1 m, 3 m, and 5 m for 1990–2019 and its difference with decades the 1990s, 2000s, and 2010s is illustrated in Fig. 9. The results reveal that probability of H_s exceeding 1 m ($P(H_s \geq 1\ \text{m})$) is more than 80% in the Northeast Atlantic Ocean and below 20% in most parts of the Arctic Ocean. We observe that there is up to ± 20 percentage points (.%) difference in $P(H_s \geq 1\ \text{m})$ between the 1990s(−)/2010s(+) and 1990–2019 in the Arctic Ocean. The probability of the significant wave height exceeding 3 m (and thus 5 m) is close to 0% in most parts of the Arctic Ocean. As expected, there is a low difference in $P(H_s \geq 1\ \text{m})$ (up to ± 5%) and a nearly no difference in $P(H_s \geq 7\ \text{m})$ between the 1990s(−)/2010s(+) and 1990–2019 in the Arctic Ocean.

The average exceedance probability of WEF for levels 20 kW m^{-1}, 40 kW m^{-1}, and 100 kW m^{-1} for 1990–2019 and its difference with decades the 1990s, 2000s, and 2010s is illustrated in Fig. 10. The results demonstrate that more than 65% of the time, WEF is higher than 20 kW m^{-1} in the Northeast Atlantic Ocean and below 10% in most parts of the Arctic Ocean. There is up to ± 10% difference in $P(WEF \geq 20\ \text{kW m}^{-1})$ between the 1990s(−)/2010s(+) and 1990–2019 in the Arctic Ocean.

For higher WEF levels, $P(WEF \geq 40\ \text{kW m}^{-1})$ and $P(WEF \geq 100\ \text{kW m}^{-1})$ are below 55% and 30% in the Northeast Atlantic, while for the Arctic Ocean, $P(WEF \geq 40\ \text{kW m}^{-1})$ and $P(WEF \geq 100\ \text{kW m}^{-1})$ are close to zero. As expected, there is a low difference in $P(WEF \geq 40\ \text{kW m}^{-1})$ (below ± 5%) and a nearly no difference in $P(H_s \geq 7\ \text{m})$ between the 1990s(−)/2010s(+) and 1990–2019 in the Arctic Ocean.

4. Discussion and concluding remarks

Our analysis results indicate that the Arctic's most energetic wave conditions are observed in the Greenland Sea and the Barents Sea due

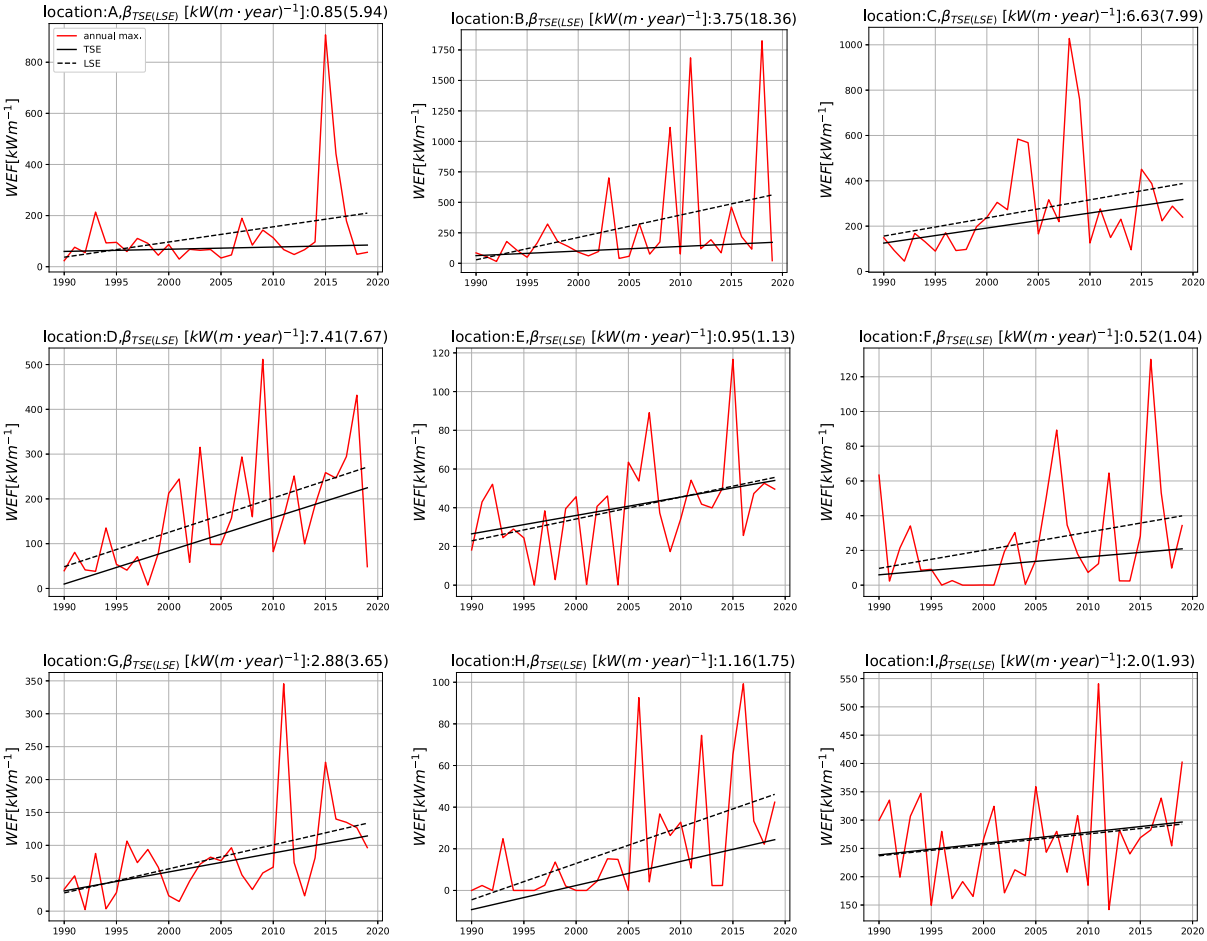

Fig. 8. Maximum annual wave energy flux (WEF) for the period January 1, 1990, to December 31, 2019, at locations A-I. The line represents the linear fit on the annual maximum values using the least-square estimator (LSE, dashed) and Theil–Sen estimator (TSE, solid).

to their direct opening to the open sea waves from the North Atlantic. However, wave energy flux should not be the sole determining factor. This study utilized the NORA3 high-resolution hindcast to further the considerations of highly energetic areas. Our approach considered accessibility and climate trends that reveal the expected persistence of the resource in the years to come.

During the last decades, the warming in the Arctic has been much more rapid than in the rest of the earth (a phenomenon known as polar or Arctic amplification). Using several datasets covering the Arctic region, Rantanen et al. [28] showed that the Arctic has been warming about four times faster than the globe during the last 43 years. The sea ice loss has a central role in Arctic amplification [29–31]. Our study shows that the substantial diminishing of sea ice in the Arctic induces local and regional changes in both average and extreme wave conditions. The reduction or vanish of sea ice creates longer or unlimited fetch, allowing the locally generated wind waves to grow while opening areas for swell waves to propagate. This indicates that wave energy applicable regions are increased and are getting more accessible year round.

When simulating the propagation of surface waves in the marginal zone, there is a source of uncertainty regarding the wave—ice scheme used in the spectral wave model. Even if there has been a significant development in the parametrizations for wave–ice interactions recently, the complexity of these interactions remains a challenge, e.g., the mechanisms that control the wave energy decay through sea ice [32]. Another uncertainty is related to the accuracy of the ice forcing for the spectral wave models. As discussed by Nose et al. [33], the uncertainty of sea ice concentration can considerably affect the performance of the spectral wave simulations in the marginal ice zone.

Extreme values, such as the annual maximum, are relevant for the metocean design basis of the marine structures/installations. The extreme value analysis is crucial for avoiding potential damages by extreme events, e.g., storms. The annual maximum values show more pronounced changes in the Arctic Ocean than mean wave conditions. Hence, waves in a storm in the 2010s have longer fetch to grow (wind sea) or area to propagate (swell) than the same storm would have in the 1990s.

The average values are important for wave energy applications and marine operations planning. The mean values represent the overall period that includes, most of the time, low-wind/calm conditions in most Arctic areas. Thus, the mean values have not changed significantly over the last decades.

The trend analysis results show that the least-squares and the Theil–Sen methods estimate similar slope values. Nevertheless, the least-squares method shows slightly higher values since it is sensitive to outliers that the studies of extreme conditions often contain. On the other hand, the Theil–Sen method uses a more robust technique of estimating the median from all slopes.

The strong positive trend in $H_{s,annual(max)}$ in the Arctic regions of the Barents Sea, the Kara Sea, the Laptev Sea, the East Siberian Sea, the Chukchi Sea, and the Beaufort Sea is an apparent effect of significant reduction of sea ice during the last decades. However, we should be cautious about the trend's magnitude in some areas, such as locations E (Laptev Sea), F (East Siberian Sea) and H (Beaufort Sea), where the annual maximum, which is close to zero for some years, shows a significant variation.

The probability of exceedance in H_s and WEF are essential parameters for the design/operation of the marine structures and wave

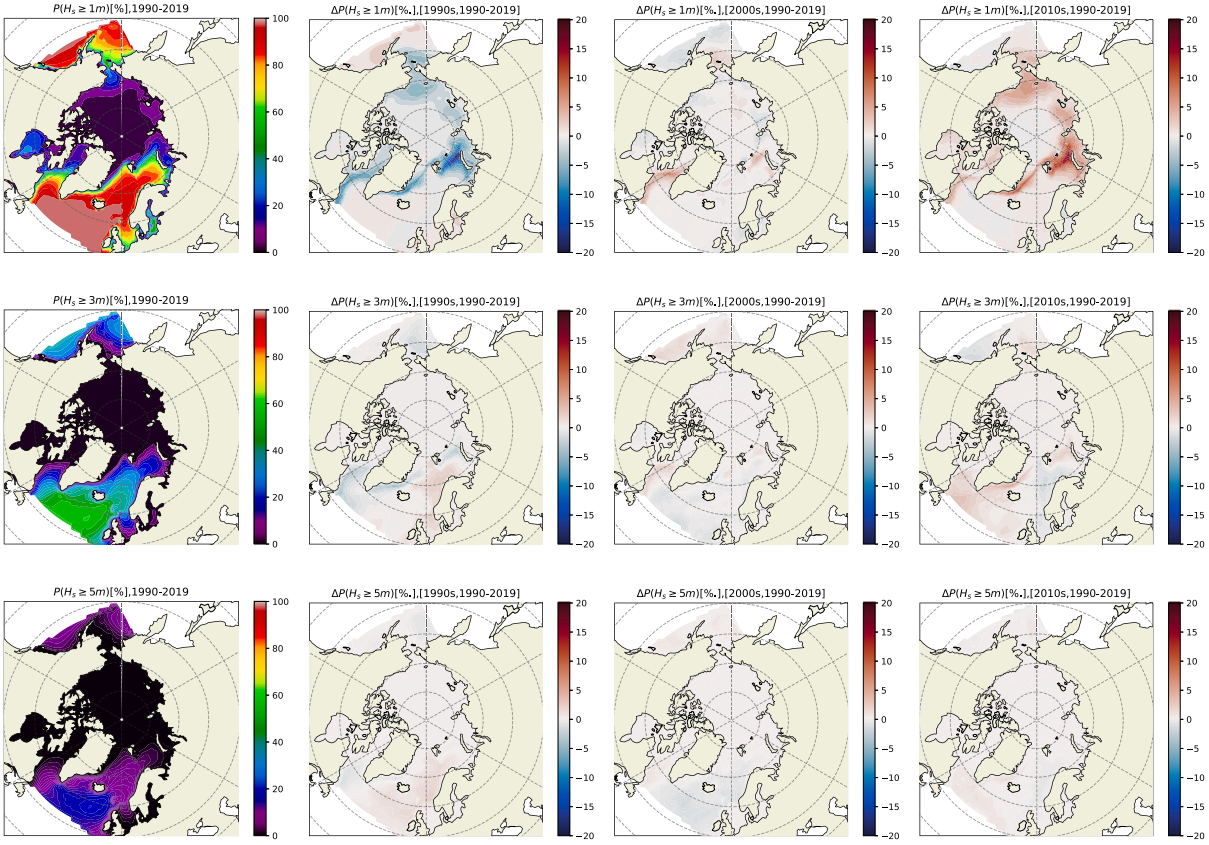

Fig. 9. Average exceedance probability of H_s for levels 1 m, 3 m, and 5 m for 1990–2019 and its difference with the 1990s, 2000s, and 2010s.

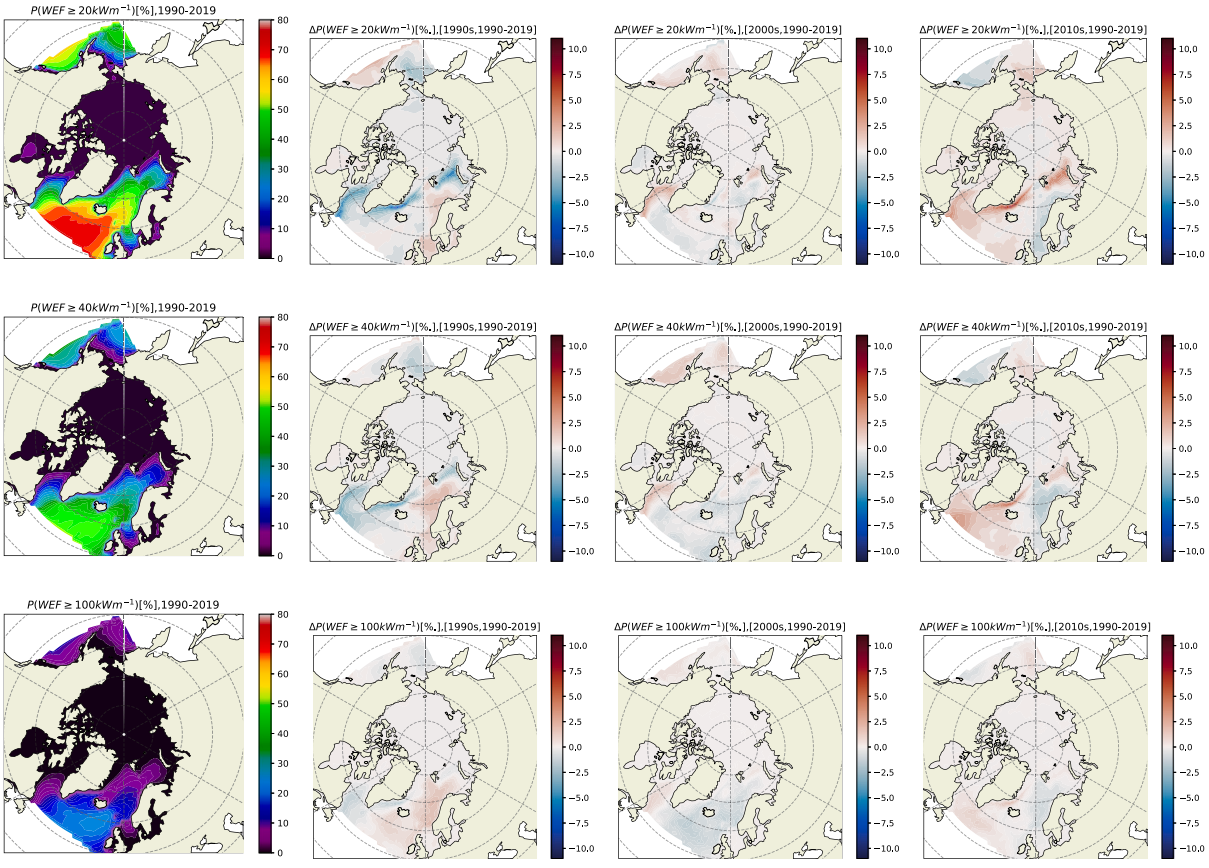

Fig. 10. Average exceedance probability of WEF for levels 20 $\mathrm{kWm^{-1}}$, 40 $\mathrm{kWm^{-1}}$, and 100 $\mathrm{kWm^{-1}}$ for 1990–2019 and its difference with the 1990s, 2000s, and 2010s.

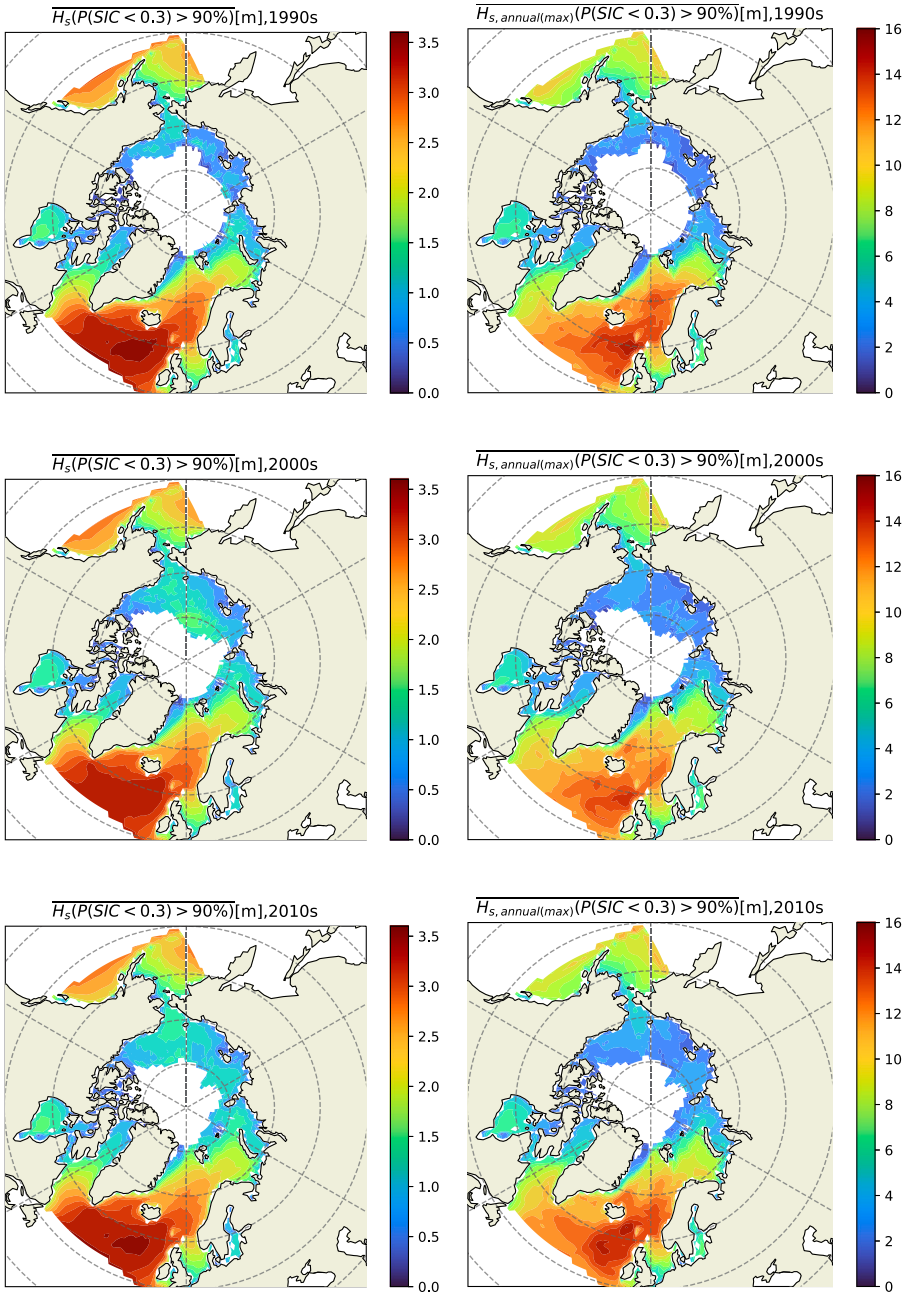

Fig. A.1. Average significant wave height ($\overline{H}_s$) and average annual maximum significant wave height ($\overline{H}_{s,annual(max)}$) for ice free conditions, i.e., probability of $SIC < 0.3$ surpassing 90% ($P(SIC < 0.3) > 90\%$) for 1990s, 2000s, and 2010s.

energy applications, respectively. The probability of H_s/WEF exceeding 1 m/20 kW^{-1} shows a substantial change (up to 20%./10%.) in some regions in the Arctic during the last decade. Marine structures' design and operation are far more complex in a rapidly changing arctic environment than in non-arctic regions where nearly no change in probability of exceedance is observed over the decades. To consider the changes in the Arctic, long-term datasets that include future climate projections are recommended for structural design, marine operations and wave energy applications.

In terms of WEF in the Arctic Sea the range of the overall mean is relative low i.e., 5 to 30 kW/m, compared to e.g., the Norwegian Sea. However, there are areas such as the Greenland Sea, the Barents Sea, and the Kara Sea which show a large variation in mean WEF, up to +8 kW/m, between 2010s and 1990–2019. This means that the region should anticipate a persistent and increased resource profile annually. On the other hand, the maxima values in the region show an increase, which needs to be considered in the deployment of marine renewable energies. This is important as it will move the expected return wave values upwards, affecting the survivability.

In the future, it will be interesting to investigate the behavior of different wave energy assessment metrics [2,3] in a rapidly changing environment of the Arctic Ocean. Furthermore, it will be valuable to investigate the effect of climate change on the design/operations of marine structures using high-resolution climate projections through downscaling the NORA3 dataset.

CRediT authorship contribution statement

Konstantinos Christakos: Conceptualization, Methodology, Software, Formal analysis, Investigation, Data curation, Writing – original draft, Writing – review & editing, Visualization. **George Lavidas:** Conceptualization, Methodology, Writing – review & editing. **Zhen Gao:**

Methodology, Writing – review & editing, Project administration, Funding acquisition. **Jan-Victor Björkqvist:** Methodology, Writing – review & editing.

Declaration of competing interest

The authors declare that they have no known competing financial interests or personal relationships that could have appeared to influence the work reported in this paper.

Acknowledgments

We want to thank Ole Johan Aarnes for his valuable comments and discussions on the extreme wave conditions at the early stage of this study. The Research Council of Norway supported this work through the center for research-based innovation SFI BLUES - Floating structures for the next generation ocean industries (https://sfiblues.no/), grant number 309281. The NORA3 data is available via the Thredds Service at the Norwegian Meteorological Institute, https://thredds.met.no.

Appendix. Figures

See Fig. A.1.

References

[1] EUROPEAN COMMISSION, An EU Strategy to Harness the Potential of Offshore Renewable Energy for a Climate Neutral Future, Tech. rep., European Commission, Brussels, 2020, URL https://eur-lex.europa.eu/legal-content/EN/TXT/?uri=COM:2020:741:FIN.

[2] N. Guillou, G. Lavidas, G. Chapalain, Wave energy resource assessment for exploitation-A review, 2020.

[3] G. Lavidas, Selection index for wave energy deployments (SIWED): A near-deterministic index for wave energy converters, Energy 196 (2020).

[4] L. Cavaleri, L. Bertotti, P. Pezzutto, Accuracy of altimeter data in inner and coastal seas, Ocean Sci. 15 (2) (2019).

[5] K. Christakos, G. Varlas, I. Cheliotis, C. Spyrou, O.J. Aarnes, B.R. Furevik, Characterization of wind-sea- and swell-induced wave energy along the Norwegian Coast, Atmosphere 11 (2) (2020) URL https://www.mdpi.com/2073-4433/11/2/166.

[6] H. Haakenstad, Ø. Breivik, B.R. Furevik, M. Reistad, P. Bohlinger, O.J. Aarnes, Nora3: A nonhydrostatic high-resolution hindcast of the North Sea, the Norwegian Sea, and the Barents sea, J. Appl. Meteorol. Climatol. 60 (10) (2021).

[7] Ø. Breivik, A. Carrasco, H. Haakenstad, O.J. Aarnes, A. Behrens, J.-R. Bidlot, J.-V. Björkqvist, P. Bohlinger, B.R. Furevik, J. Staneva, M. Reistad, The impact of a reduced high-wind charnock parameter on wave growth with application to the North Sea, the Norwegian Sea, and the Arctic Ocean, J. Geophys. Res.: Oceans 127 (3) (2022) e2021JC018196, URL https://agupubs.onlinelibrary.wiley.com/doi/abs/10.1029/2021JC018196.

[8] H. Hersbach, B. Bell, P. Berrisford, S. Hirahara, A. Horányi, J. Muñoz-Sabater, J. Nicolas, C. Peubey, R. Radu, D. Schepers, A. Simmons, C. Soci, S. Abdalla, X. Abellan, G. Balsamo, P. Bechtold, G. Biavati, J. Bidlot, M. Bonavita, G. De Chiara, P. Dahlgren, D. Dee, M. Diamantakis, R. Dragani, J. Flemming, R. Forbes, M. Fuentes, A. Geer, L. Haimberger, S. Healy, R.J. Hogan, E. Hólm, M. Janisková, S. Keeley, P. Laloyaux, P. Lopez, C. Lupu, G. Radnoti, P. de Rosnay, I. Rozum, F. Vamborg, S. Villaume, J.N. Thépaut, The ERA5 global reanalysis, Q. J. R. Meteorol. Soc. 146 (730) (2020) 1999–2049.

[9] M. Müller, M. Homleid, K.-I. Ivarsson, M.A.O. Køltzow, M. Lindskog, K.H. Midtbø, U. Andrae, T. Aspelien, L. Berggren, D. Bjørge, P. Dahlgren, J. Kristiansen, R. Randriamampianina, M. Ridal, O. Vignes, AROME-MetCoOp: A Nordic Convective-Scale Operational Weather Prediction Model, Weather Forecast. 32 (2) (2017) 609–627, URL http://dx.doi.org/10.1175/WAF-D-16-0099.1.

[10] G.J. Komen, L. Cavaleri, M. Donelan, K. Hasselmann, S. Hasselmann, P.A.E.M. Janssen, Dynamics and Modelling of Ocean Waves, Cambridge University Press, Cambridge, 1994.

[11] H. Guenther, S. Hasselmann, P. Janssen, The WAM Model Cycle 4, Tech. rep., Deutsches KlimaRechenZentrum, Hamburg, Germany, 1992.

[12] The Wamdi Group, The WAM model - a third generation ocean wave prediction model, J. Phys. Oceanogr. 18 (12) (1988) 1775–1810.

[13] Copernicus Marine Service, Arctic – monitoring forecasting centre (ARC MFC): CMEMS, 2023, URL https://marine.copernicus.eu/about/producers/arctic-mfc.

[14] J. Xie, L. Bertino, L. Knut, P. Sakov, Quality assessment of the TOPAZ4 reanalysis in the Arctic over the period 1991–2013, 2017.

[15] F. Ardhuin, E. Rogers, A.V. Babanin, J.F. Filipot, R. Magne, A. Roland, A. van der Westhuysen, P. Queffeulou, J.M. Lefevre, L. Aouf, F. Collard, Semiempirical dissipation source functions for ocean waves. Part I: Definition, calibration, and validation, J. Phys. Oceanogr. 40 (9) (2010) 1917–1941.

[16] L. Tuomi, H. Pettersson, C. Fortelius, K. Tikka, J.V. Björkqvist, K.K. Kahma, Wave modelling in archipelagos, Coast. Eng. 83 (2014).

[17] EMODnet Bathymetry Consortium, EMODnet digital bathymetry (DTM 2018), 2018, URL http://dx.doi.org/10.12770/18ff0d48-b203-4a65-94a9-5fd8b0ec35f6.

[18] L. Tuomi, K.K. Kahma, H. Pettersson, Wave hindcast statistics in the seasonally ice-covered Baltic sea, Boreal Environ. Res. 16 (6) (2011).

[19] H.L. Tolman, Treatment of unresolved islands and ice in wind wave models, Ocean Model. 5 (3) (2003).

[20] L. Tuomi, H. Kanarik, J.V. Björkqvist, R. Marjamaa, J. Vainio, R. Hordoir, A. Höglund, K.K. Kahma, Impact of ice data quality and treatment on wave hindcast statistics in seasonally ice-covered seas, Front. Earth Sci. 7 (2019).

[21] G. Sutherland, J. Rabault, K.H. Christensen, A. Jensen, A two layer model for wave dissipation in sea ice, Appl. Ocean Res. 88 (2019).

[22] G. Lavidas, A. Agarwal, V. Venugopal, Availability and accessibility for offshore operations in the Mediterranean Sea, J. Waterw. Port Coast. Ocean Eng. 144 (6) (2018).

[23] M. O'Connor, T. Lewis, G. Dalton, Weather window analysis of irish west coast wave data with relevance to operations & maintenance of marine renewables, Renew. Energy 52 (2013).

[24] P.K. Sen, Estimates of the regression coefficient based on Kendall's tau, J. Amer. Statist. Assoc. 63 (324) (1968).

[25] H.B. Mann, Nonparametric tests against trend, Econometrica 13 (3) (1945).

[26] M.G. Kendall, Rank Correlation Methods, Oxford University Press, 1975.

[27] M. Hussain, I. Mahmud, pyMannKendall: a python package for non parametric mann Kendall family of trend tests, J. Open Source Softw. 4 (39) (2019).

[28] M. Rantanen, A.Y. Karpechko, A. Lipponen, K. Nordling, O. Hyvärinen, K. Ruosteenoja, T. Vihma, A. Laaksonen, The arctic has warmed nearly four times faster than the globe since 1979, Commun. Earth Environ. 3 (1) (2022).

[29] J.A. Screen, I. Simmonds, The central role of diminishing sea ice in recent arctic temperature amplification, Nature 464 (7293) (2010).

[30] M. Jenkins, A. Dai, The impact of sea-ice loss on arctic climate feedbacks and their role for Arctic amplification, Geophys. Res. Lett. 48 (15) (2021).

[31] A. Dai, D. Luo, M. Song, J. Liu, Arctic amplification is caused by sea-ice loss under increasing CO 2, Nature Commun. 10 (1) (2019).

[32] J. Thomson, S. Ackley, F. Girard-Ardhuin, F. Ardhuin, A. Babanin, G. Boutin, J. Brozena, S. Cheng, C. Collins, M. Doble, C. Fairall, P. Guest, C. Gebhardt, J. Gemmrich, H.C. Graber, B. Holt, S. Lehner, B. Lund, M.H. Meylan, T. Maksym, F. Montiel, W. Perrie, O. Persson, L. Rainville, W. Erick Rogers, H. Shen, H. Shen, V. Squire, S. Stammerjohn, J. Stopa, M.M. Smith, P. Sutherland, P. Wadhams, Overview of the Arctic sea state and boundary layer physics program, J. Geophys. Res.: Oceans 123 (12) (2018).

[33] T. Nose, T. Waseda, T. Kodaira, J. Inoue, Satellite-retrieved sea ice concentration uncertainty and its effect on modelling wave evolution in marginal ice zones, Cryosphere 14 (6) (2020) 2029–2052.